ÉCOLE POLYTECHNIQUE FÉDÉRALE DE LAUSANNE
MATHICSE
Institute of Mathematics
School of Basic Sciences

MATHICSE Technical Report
Nr. 06.2018
April 2018

A continuation-multilevel Monte Carlo evolutionary algorithm for robust aerodynamic shape design

Michele Pisaroni, Fabio Nobile, Penelope Leyland

https://math.epfl.ch/h

Address: EPFL - SB – INSTITUTE of MATHEMATICS – Math
(Bâtiment MA) Station 8 - CH-1015 - Lausanne - Switzerland

A Continuation-Multilevel Monte Carlo Evolutionary Algorithm for Robust Aerodynamic Shape Design

Michele Pisaroni[a], Fabio Nobile[a], Penelope Leyland[a]

[a] *École polytechnique fédérale de Lausanne, MATH CSQI, Station 8, 1015 Lausanne, Switzerland*

Abstract

The majority of problems in aircraft production and operation require decisions made in the presence of uncertainty. For this reason aerodynamic designs obtained with traditional deterministic optimization techniques seeking only optimality in a specific set of conditions may have very poor off-design performances or may even be unreliable. In this work, we present a novel approach for robust and reliability-based design optimization of aerodynamic shapes based on the combination of single and multi-objective Evolutionary Algorithms and a Continuation Multi Level Monte Carlo methodology to compute objective functions and constraints that involve statistical moments or statistical quantities such as quantiles, also called Value at risk, (VaR) and Conditional Value at Risk (CVaR) without relying on derivatives and meta-models. Detailed numerical studies are presented for the RAE-2822 transonic airfoil design affected by geometrical and operational uncertainties.

Keywords: Multi Level Monte Carlo, Uncertainty Quantification, Aerodynamic Design, Robust Design Optimization, Evolutionary Algorithms.

1. Introduction

In the early days of aviation, the limitations due to propeller propulsion avoided airplanes from flying fast enough to encounter transonic/supersonic phenomena. During the Second World War fighters started reaching transonic speeds and encountered major difficulties in recovering from dives during maneuvering, controllability issues related to sharp pitching moment changes with the Mach number and Mach induced changes in control effectiveness. Since the introduction of jet engines in civil aviation, practically all commercial transport aircrafts now fly at transonic speeds. Transonic conditions occur during a flight when there are subsonic and supersonic local flows in the same flow field surrounding an aircraft. Generally, this happens in a range of speeds between the so called *critical Mach number* (around Mach 0.72), when some parts of the airflow start becoming supersonic, and the speed when all of the airflow is supersonic (around Mach 1.05 in conventional airfoils). At transonic speed, the supersonic regions of the flow are generally followed by a shock wave, that slows down the flow to subsonic conditions. The fuel consumption due to rapid increase of wave and viscous drag with the Mach number (shocks get stronger and pressure rise through a shock wave thickens the boundary layer) typically limits the cruise speed of commercial aircrafts.

Notwithstanding it is possible to design a shock free airfoil, this situation usually takes place only for a single combination of Mach number and lift coefficient. For this reason, much effort has been spent since the 1960s, following the pioneering work of Whitcomb on supercritical airfoil [1], to reduce the shock drag and increase the controllability in a range of Mach number without fully suppressing the shocks. Supercritical airfoils were designed to achieve higher drag rise Mach numbers by controlling the expansion of the flow to supersonic speed and its subsequent recompression without affecting the lifting performances. Supercritical

*Corresponding author
Email address: michele.pisaroni@epfl.ch (Michele Pisaroni)

airfoils generally present a relatively large leading edge radius to expand the flow in the upper surface and obtain more lift than conventional airfoils in the bow part (region near the leading edge). In addition, a flatter upper surface, compared to conventional airfoils, maintains the supersonic flow at nearly a constant pressure plateau or even slows it down slightly approaching the shock. Thanks to that, a relatively weak shock is produced. In some cases also an augmented aft camber (region near the trailing edge) can be employed to produce more lift than conventional airfoils.

Although theoretically superior with respect to conventional airfoils, promising supercritical sections led to serious problems when actually incorporated into an aircraft wing. Practical experiences revealed that some supercritical sections, with shock-free designs, are often very sensitive to Mach, lift and geometrical uncertainties and hence may perform dramatically poorly at off-design conditions. Optimizing a transonic airfoil shape using classical deterministic optimization methodologies seeking optimality only in a single operating condition generally leads to the appearance of the so called *drag creep*, a situation in which the drag increases at Mach numbers below the designed value. On the other hand, multi-point optimization approaches, seeking optimality in multiple discrete operating points can alleviate the drag creep phenomenon but are unable to adequately remedy the problem of localized optimization [2] (i.e. shapes that are optimal in only few operating conditions, generally characterized by few bumps).

The ever-increasing demand for aircrafts with better performance, higher reliability and robustness at lower cost requires optimization techniques seeking optimality under uncertain conditions that may arise during design, manufacture and operation of the vehicle. Indeed, the geometrical and operational parameters, that characterize aerodynamic systems, are naturally affected by aleatory uncertainties due to the intrinsic variability of the manufacturing processes and the surrounding environment. Reducing the geometrical uncertainties due to manufacturing tolerances can be prohibitively expensive while reducing the operational uncertainties due to atmospheric turbulence in external aerodynamics is simply impossible.

Optimization under uncertainty (OUU) refers to a broad class of methodologies that address the following two problems:

- Robust Design Optimization (RDO): focuses on the performances of a system under perturbations of the design conditions. Prescribed probabilistic measures of robustness (involving mean, variance or higher moments) as objective functions are used to "robustify" the design. The optimal design should, in this framework, be as insensitive as possible to uncertain conditions meaning that its performance should not drop below a prescribed quality level. The final objective of RDO is to achieve an improvement of the performance of the system over the entire range of uncertain conditions [3] by reducing the performance variability (a graphical interpretation of RDO is provided in Figure 1(a)).

- Reliability-based Design Optimization (RBDO): focuses on safety-under-uncertainty aspects of the system. The most conservative and classical approach for RBDO is the worst-case analysis (also known as min-max strategy) that seeks a design with the best "worst-case" performance [4]. More modern and advanced methodologies seek the optimization of an objective functions subject to probabilistic constraints that involve failure probabilities (such as quantiles and Conditional Value at Risk - CVaR) or reliability indexes. The optimal design has, in this framework, a prescribed degree of confidence and a minimum level of reliability under uncertain conditions (a graphical interpretation of RBDO is provided in Figure 1(b)).

Despite the wide availability of modern parallel computer architectures and efficient CFD solvers, the key difficulties in RDO/RBDO problems are:

- computing objective functions that involve robust measures based on mean, variances and higher moments or reliability measures such as VaR and CVaR, when many sources of uncertainties are present (efficient propagation of uncertainties).

- dealing with competing objectives in computing a robust Pareto-optimal front.

Many non-intrusive uncertainty propagation techniques and derivatives-free optimization method have gained a lot of attention in recent years as they simply require multiple solutions of the original problem and

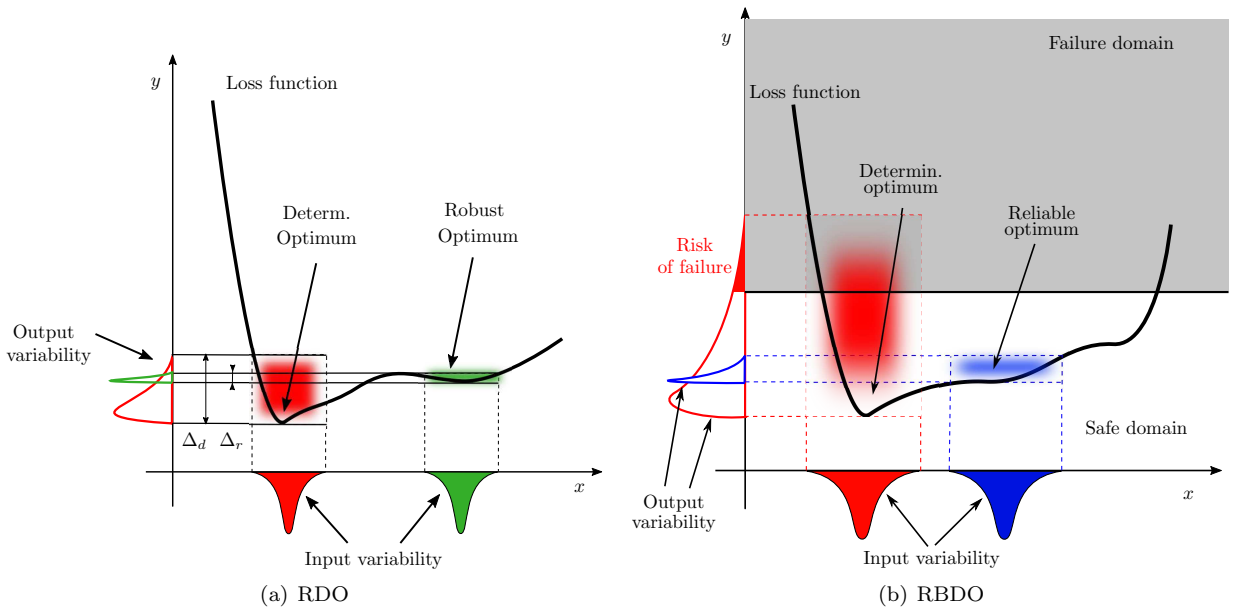

Figure 1: Graphical interpretation of robust design optimization (RDO), left and reliability-based design optimization (RBDO), right. The green (resp. the blue) design is more robust (resp. reliable) than the red one. In this graphical representation, uncertainty is present on the design variable itself, i.e. the actual design is a random perturbation of the nominal one.

can use available industrial CFD solvers as a black box. Polynomial Chaos (PC) [5, 6, 7] and Stochastic Collocation (SC) [8] methods have been successfully employed in different engineering fields to built response surfaces of the system outputs with respect to the uncertain parameters to be used in the optimization loop, while Kriging [9] has been mainly employed to build meta-models for the system response with respect to the design variables. All these approaches have a strong potential for RDO but they are known to suffer the so called 'curse of dimensionality' (dramatically increase of computational cost with the number of uncertain/design variables). In addition, these approaches based on global basis functions that span the entire stochastic design domain may see their performance and accuracy jeopardized if the problem under investigation presents strong discontinuities as in the case of transonic/supersonic flows.

Monte Carlo (MC) methods, on the contrary, have been proven to be robust and accurate for non smooth problems. However, their very slow convergence rate, although dimension independent, makes them chimerical for practical applications. The Multi Level Monte Carlo (MLMC) method, introduced by Heinrich [10] and Giles [11] is based on the intuitive idea that one can draw MC samples simultaneously and independently on several approximations of the problem under investigations on a hierarchy of nested computational grids (levels). In a previous work we presented a robust and effective Continuation Multi Level Monte Carlo (C-MLMC) methodology [12], following the ideas of Collier et al.[13], which is capable of propagating operational and geometrical uncertainties in compressible inviscid flow problems and allows an effective reduction of the overall computational efforts compared to MC and classical MLMC. In [14] we introduced an extension of the standard MLMC approach to compute arbitrary order central statistical moments.

In this work we present an effective procedure that leverages the self-tuning nature and robustness of C-MLMC to compute robust/reliable loss function and constraints that involve statistical moments and generalized quantiles (value at risk, VaR and conditional value at risk CVaR) combined with a Covariance Matrix Adaptation Evolutionary Strategy (CMA-ES) to solve the optimization problem. The approach is tested and applied in different settings relevant in airfoil design: single objective maximization of lift-drag ratio with uncertainties in operating and geometric conditions (up to 10 uncertain parameters), minimization of drag coefficient with uncertainties in the operating conditions and multi objective optimization of lift and

drag coefficients with operating and geometric uncertainties.

The paper is organized as follows. Section 2 introduce the notations and the formulation of deterministic airfoil optimization problems, Section 3 presents the problem of optimization under uncertainties and robust and reliability-based loss functions and constraints relevant in airfoil design. Section 4 introduce the Continuation-MLMC Evolutionary algorithm. Section 5 presents the application of the algorithm to single-objective optimization under uncertainties and Section 6 the application of the algorithm to multi-objective optimization problems. Section 7 concludes the paper and proposes future work.

2. Deterministic Shape Optimization

In a deterministic framework, a single objective (SO) airfoil shape optimization problem consists of determining the set of geometric design parameters χ that minimize (or maximize) a prescribed deterministic loss (or fitness in case of maximization) function $\mathcal{D} : \mathbb{R}^q \to \mathbb{R}$

$$\text{SO-DO} : \begin{cases} \min\limits_{\chi \in \mathbb{R}^n} \ \mathcal{D}\left[\mathbf{Q}_d^q(\chi, p)\right] \\ \quad s.t \ \ \mathcal{C}_i\left[\mathbf{Q}_c^m(\chi, p)\right] \leq k_i \qquad i = 1, \ldots, s \\ \qquad \chi_L \leq \chi \leq \chi_U \end{cases} \tag{1}$$

Here

- $\chi \in \mathbb{R}^n$ is a vector of n design variables, $\chi = (\chi_1, \ldots, \chi_n)$, that define the shape of the airfoil, and may be subject to constraints $\chi_{L,i} \leq \chi_i \leq \chi_{U,i}$. We write such constraints in compact form as $\chi_L \leq \chi \leq \chi_U$, which should be understood component-wise.
- $p \in \mathbb{R}^g$ is a vector of system parameters as, for example fixed geometric or operating parameters of the aerodynamic system under investigation.
- $\mathbf{Q}_d^q(\chi, p) = \left[Q_d^1(\chi, p), \ldots, Q_d^q(\chi, p)\right]$ is the vector of q Quantities of Interest (QoI) that enter in the expression of the objective function $\mathcal{D}$. These could be for example the lift, drag or momentum coefficient of an airfoil.
- $\mathbf{Q}_c^m(\chi, p) = \left[Q_c^1(\chi, p), \ldots, Q_c^m(\chi, p)\right]$ is the vector of m QoI that are subject to constraints, defined by the functions $\mathcal{C}_i : \mathbb{R}^m \to \mathbb{R},\ i = 1, \ldots, s$ as $\mathcal{C}_i(\mathbf{Q}_c^m) \leq k_i$.

Definition 1. *We call* feasible design set X, *the set* $X = \{\chi \in \mathbb{R}^n \mid \mathcal{C}_i\left[\mathbf{Q}_c^m(\chi, p)\right] \leq k_i, i = 1, \ldots, s$ *and* $\chi_L \leq \chi \leq \chi_U\}$

With this definition, the SO airfoil design problem can be written more compactly as $\min_{\chi \in X} \ \mathcal{D}\left[\mathbf{Q}_d^q(\chi, p)\right]$.

We now turn to a Multi Objective (MO) airfoil shape problem and define $\mathbf{D}^\Phi\left[\mathbf{Q}_d^q(\chi, p)\right]$, $\mathbf{D}^\Phi : \mathbb{R}^q \to \mathbb{R}^\Phi$ a vector of loss functions:

$$\mathbf{D}^\Phi\left[\mathbf{Q}_d^q(\chi, p)\right] = \left[\mathcal{D}_1\left[\mathbf{Q}_d^q(\chi, p)\right], \ldots, \mathcal{D}_\Phi\left[\mathbf{Q}_d^q(\chi, p)\right]\right] \tag{2}$$

Using the same notation as in (1), we define the multi-objective design optimization problem (MO-DO) as :

$$\text{MO-DO} : \begin{cases} \text{P-min}\limits_{\chi \in \mathbb{R}^n} \ \mathbf{D}^\Phi\left[\mathbf{Q}_d^q(\chi, p)\right] \\ \quad s.t \ \ \mathcal{C}_i\left[\mathbf{Q}_c^m(\chi, p)\right] \leq k_i \qquad i = 1, \ldots, s \\ \qquad \chi_L \leq \chi \leq \chi_U \end{cases} \tag{3}$$

where Φ is the number of objective functions and P-min denotes all Pareto optimal values of $\mathbf{D}^\Phi$ on the feasible set $X \subset \mathbb{R}^n$.

Definition 2. *A feasible point* $\chi^* \in X$ *is Pareto optimal if and only if there does not exist another feasible point* $\chi \in X$ *such that* $\boldsymbol{D}^\Phi\left[\mathbf{Q}_d^q(\chi, p)\right] \leq \boldsymbol{D}^\Phi\left[\mathbf{Q}_d^q(\chi^*, p)\right]$, *and* $\mathcal{D}_i\left[\mathbf{Q}_d^q(\chi, p)\right] < \mathcal{D}_i\left[\mathbf{Q}_d^q(\chi^*, p)\right]$ *for at least one* $i \in \{1, \ldots, \Phi\}$.

The main difference between SO-DO and MO-DO is that in the latter usually there is no single solution, but a set of points defining the so called "Pareto front".

In airfoil shape design, one is generally interested in minimizing the drag coefficient of the airfoil or maximizing its lift-drag ratio. Constraints are generally imposed on the geometry of the airfoil, in order to achieve a final optimized shape that fulfill specific structural and mission requirements, and/or on the lift and moment coefficient. Examples of loss functions considered in this work are provided in the following Table 1. There SP denotes deterministic single point optimization problems solved for a single flight Mach number condition, while MP denotes multi point deterministic optimization problems. We denote with $L/D^{(M_\infty,\alpha_\infty)}$, $C_D^{(M_\infty,\alpha_\infty)}$ and $C_L^{(M_\infty,\alpha_\infty)}$ the lift-drag ratio, the drag coefficient and lift coefficient of the airfoil at prescribed Mach number M_∞ and angle of attack α_∞. $C_D^{(M_\infty,C_L^*)}$ denotes instead the drag coefficient at prescribed Mach number M_∞ and cruise lift coefficient C_L^*.

	Loss Functions
SO (SP)	$\mathcal{D}\left[L/D\right] = L/D^{(M_\infty,\alpha_\infty)}$
SO (SP)	$\mathcal{D}\left[C_D\right] = C_D^{(M_\infty,C_L^*)}$
SO (MP)	$\mathcal{D}\left[C_D^w\right] = \sum_{i=1}^{m} w_i \cdot C_d^{(M_\infty^i,C_L^*)}$
MO	$\mathbf{D}^2\left[C_D, C_L\right] = \{C_D^{(M_\infty,\alpha_\infty)}, C_L^{(M_\infty,\alpha_\infty)}\}$

Table 1: Examples of deterministic loss functions for airfoil shape optimization problems.

3. Shape Optimization Under Uncertainties

A general formulation of a single objective optimization problem under uncertainties (SO-OUU) reads as follows:

$$\text{SO-OUU}: \begin{cases} \min\limits_{\chi\in\mathbb{R}^n} & \mathcal{R}\left[\mathbf{Q}_r^q(\widetilde{\chi}(\chi,\omega),p(\omega))\right] \\ s.t & \mathcal{C}_i\left[\mathbf{Q}_c^m(\widetilde{\chi}(\chi,\omega),p(\omega))\right] \leq k_i \qquad i=1,\ldots,s \\ & \chi_L \leq \chi \leq \chi_U \end{cases} \tag{4}$$

Here

- $\chi \in \mathbb{R}^n$ is a vector of n design variables, that define the shape of the airfoil. Its actual realization $\widetilde{\chi}(\chi,\omega)$ may be affected by uncertainties denoted as $\omega \in \Omega$, where Ω is the sample space.
- $p \in \mathbb{R}^g$ is the vector of system parameters and may also be affected by uncertainties $\omega \in \Omega$.
- $\mathbf{Q}_r^q(\widetilde{\chi}(\chi,\omega),p(\omega)) = \left[Q_r^1(\widetilde{\chi}(\chi,\omega),p(\omega)),\ldots,Q_r^q(\widetilde{\chi}(\chi,\omega),p(\omega))\right]$ is the vector of q QoI affected by uncertainty that enter in the robust loss function.
- $\mathbf{Q}_c^m(\widetilde{\chi}(\chi,\omega),p(\omega)) = \left[Q_c^1(\widetilde{\chi}(\chi,\omega),p(\omega)),\ldots,Q_c^m(\widetilde{\chi}(\chi,\omega),p(\omega))\right]$ is the vector of m QoI affected by uncertainty that are subject to s constraints.
- $\mathcal{R}$ is a robust loss function (or fitness in case of maximization) involving one or more QoI Q_r (e.g. weighted sum) that has to be optimized.
- $\mathcal{C}_i$, $i = 1,\cdots,s$, denotes a set of deterministic or probabilistic constraints applied on the set of QoI $\mathbf{Q}_c^m$.

The loss function $\mathcal{R}$ is a measure of robustness/reliability against the uncertainties in the design and system parameters. Classical robust optimization approaches generally consider optimizing performance under 'worst-case' outcomes (min-max formulations). This approach is known to generally produce overly conservative designs with suboptimal performance in the uncertainty range. In this work we consider instead

different probabilistic loss functions and constraints that involve the weighted sums of central statistical moments, Value at Risk (VaR) and Conditional Value at Risk (CVaR) of the quantities of interest that have to be optimized.

In a multi objective optimization problem under uncertainties (MP-OUU), we define with $\mathbf{R}^{\Phi}\left[\mathbf{Q}_r^q(\widetilde{\chi}(\chi,\omega),p(\omega))\right]$ a vector of Φ robust loss functions:

$$\mathbf{R}^{\Phi}\left[\mathbf{Q}_r^q(\widetilde{\chi}(\chi,\omega),p(\omega))\right] = \left[\mathcal{R}_1\left[\mathbf{Q}_r^q(\widetilde{\chi}(\chi,\omega),p(\omega))\right],\ldots,\mathcal{R}_{\Phi}\left[\mathbf{Q}_r^q(\widetilde{\chi}(\chi,\omega),p(\omega))\right]\right] \tag{5}$$

We can now further generalize (4) and define the multi-objective robust optimization problem under uncertainties (MO-OUU) as :

$$\text{MO-OUU}: \begin{cases} \underset{\chi\in\mathbb{R}^n}{\text{P-min}} \;\; \mathbf{R}^{\Phi}\left[\mathbf{Q}_r^q(\widetilde{\chi}(\chi,\omega),p(\omega))\right] \\ \quad s.t \;\; \mathcal{C}_i\left[\mathbf{Q}_c^m(\widetilde{\chi}(\chi,\omega),p(\omega))\right] \leq k_i \qquad i=1,\ldots,s \\ \quad\quad \chi_L \leq \chi \leq \chi_U \end{cases} \tag{6}$$

where Φ is the number of objective functions and P-min denote all Pareto optimal values of $\mathbf{R}^{\Phi}$ over X.

Examples of probabilistic (robust and reliable) loss functions considered in this work are provided in the following Table 2. There μ, σ and VaR^{90} respectively denote the mean, standard deviation and Value at Risk (VaR, i.e. 90% quantile) of a specific QoI affected by operating and/or geometric uncertainties.

	Probabilistic Loss Functions
$\mathcal{R}_{\mu,\sigma}\left[C_D\right]$	$\mu_{C_D}+\sigma_{C_D}$
$\mathcal{R}_{VaR^{90}}\left[C_D\right]$	$VaR^{90}_{C_D}$
$\mathbf{R}^2\left[C_D,C_L\right]$	$\{\mu_{C_D}+\sigma_{C_D},\mu_{C_L}-\sigma_{C_L}\}$

Table 2: Examples of probabilistic loss functions for airfoil shape optimization problems under uncertainties.

3.1. Airfoil Parametrization

In this work we use as design parameters the set of PARSEC parameters or the position of control box nodes for a Free Form Deformation (FFD) box.

3.1.1. PARSEC

The PARSEC approach is a constructive parametrization methodology proposed by Sobieczky [15] to introduce engineering relevant and geometrically intuitive airfoil parameters in the design process. In a 2D plane x-y, the suction and pressure sides of the airfoil shape are defined as the graph of functions $y_s(x)$ and $y_p(x)$, respectively, with the following form:

$$y_s(x)=\sum_{i=0}^{6} s_i x^{i-0.5}, \qquad y_p(x)=\sum_{i=0}^{6} p_i x^{i-0.5}, \qquad x\in[0,1] \tag{7}$$

The free parameters are the PARSEC parameters presented in Table 3 together with their relation with the coefficients $\{s_i\}$ and $\{p_i\}$. The shape of the airfoil (7) is then determined by solving the set of 12 (nonlinear) equations for the coefficients s_i and p_i, $i=1,\ldots,6$ given the PARSEC parameters (see right column of Table 3).

It is worth underlying that in our framework we set the trailing edge offset Y_{TE} and the trailing edge thickness ΔY_{TE} to zero. Hence the airfoil shapes are identified by 10 parameters as presented in figure 2(a).

Parameter	Symbol	Definition
Pressure LE radius	R_p	p_1
Suction LE radius	R_s	s_1
Pressure Crest position	X_p	$y'_p(X_p) = 0$
Suction Crest position	X_s	$y'_s(X_s) = 0$
Pressure Crest hight	Y_p	$y_p(X_p)$
Suction Crest hight	Y_s	$y_s(X_s)$
Pressure Crest curvature	C_p	$y''_p(X_p)$
Suction Crest curvature	C_s	$y''_s(X_s)$
TE angle	θ_s	$y'_s(1) = -tan(\theta_s + \frac{\theta_p}{2})$
Boat-tail angle	θ_p	$y'_p(1) = -tan(\theta_s - \frac{\theta_p}{2})$
TE offset	Y_{TE}	$y_p(1)$
TE thickness	ΔY_{TE}	$y_s(1) - y_p(1)$

Table 3: PARSEC parameters and definitions (LE= leading edge; TE= trailing edge).

3.1.2. Free-Form Deformation (FFD)

The FFD methodology has been first introduced as a computer graphics 3D morphing technique [16] and afterwards proposed in the context of aerodynamic optimization [17]. The approach is based on the intuitive idea of expressing the deformation from an initial nominal shape by the displacement of an embedding control box. The competitive advantage of this approach is that, as the external box is deformed, the embedded objects are deformed too with the same degree of flexibility. This is particularly appealing when the FFD approach is applied on CFD grid boundaries. The airfoil/wing shape and the computational grid surrounding it can be smoothly deformed in just one step.

Considering the local curvilinear coordinates $\boldsymbol{x} = (s, t, u)$ mapped into the control box (lattice coordinates), the displacement $\delta(\boldsymbol{x})$ of any point inside the control box is defined as:

$$\boldsymbol{x} + \delta(\boldsymbol{x}) = \sum_{i=1}^{l}\sum_{j=1}^{m}\sum_{k=1}^{n} \boldsymbol{B}_{l-1}^{i-1}(s)\boldsymbol{B}_{m-1}^{j-1}(t)\boldsymbol{B}_{n-1}^{k-1}(u)\,(\boldsymbol{P}_{i,j,k} + \boldsymbol{D}_{i,j,k}) \tag{8}$$

where $\boldsymbol{B}_{l-1}^{i-1}(s)$ is the $(i-1)$-th Bernstein polynomial of degree $l-1$ [18]. $\boldsymbol{P}_{i,j,k}$ and $\boldsymbol{D}_{i,j,k}$ are the matrices of original coordinates and displacements for the node points (i, j, k) of the control box lattice defined by $n_{cp} = l \cdot m \cdot n$ control points (see Figure 2(b)).

Starting from the local curvilinear coordinates of the points embedded by the control box and the blending functions $\boldsymbol{B}$, once the external box is deformed (update of $\boldsymbol{D}_{i,j,k}$), the location of all nodes inside it are obtained from (8).

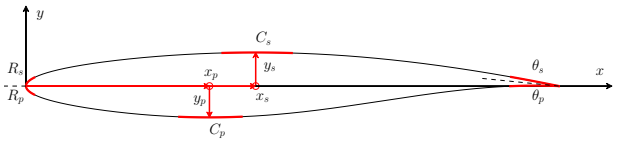

(a) PARSEC parametrization for RAE2822

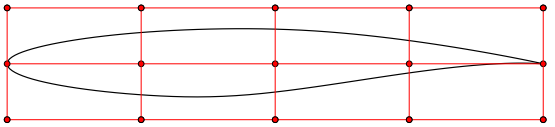

(b) FFD box for RAE2822

Figure 2: PARSEC and FFD parametrization for the RAE-2822 airfoil.

4. Continuation Multilevel Monte Carlo Evolutionary Algorithm

In this work we employ Single and Multi Objective Covariance Matrix Adaptation Evolutionary Strategies (CMA-ES) to solve the SO-OUU and MO-OUU problems presented above. We hereafter introduce the general idea of CMA-ES and we then introduce the modifications required to treat optimization problems under uncertainty by means of the Continuation Multi Level Monte Carlo (C-MLMC) technique. Finally, we present the full C-MLMC CMA-ES algorithm.

4.1. Covariance Matrix Adaptation Evolutionary Strategies (CMA-ES)

CMA-ES are a class of stochastic derivative-free evolutionary algorithms for numerical optimization of non-linear and non-convex black-box optimization problems introduced by Hansen [19].

Based on the principle of biological evolution, evolutionary algorithms, are characterized by the repeated interplay of variation and selection operators. At each generation (iteration of the algorithm) new individuals (candidate solutions) are generated by variation of the current parental individuals via recombination and possibly mutation. The individuals with the best fitness (objective function value) are then selected and become the parents in the next generation. Thanks to this repeated process, individuals with increasingly better fitness are generated.

In classical ES a new population of $\lambda \geq 2$ candidate solutions at generation $i+1$ is sampled according to a multivariate normal distribution in $\mathbb{R}^n$, n being the number of design variables, as

$$\chi_k^{(i+1)} \sim m^{(i)} + \sigma^{(i)} \mathcal{N}(0, C^{(i)}) \sim \mathcal{N}(m^{(i)}, (\sigma^{(i)})^2 C^{(i)}) \qquad \textbf{for} \qquad k = 1, \ldots, \lambda \tag{9}$$

where $\chi_k^{(i+1)} \in \mathbb{R}^n$ denotes the k-th individual in generation $i+1$, $m^{(i)} \in \mathbb{R}^n$ the mean of the population at generation i, $C^{(i)} \in \mathbb{R}^{n \times n}$ is a scaled covariance matrix of the population at generation i and $\sigma^{(i)} \in \mathbb{R}$ is a scaling parameter (step-size).

The **recombination** operator is responsible for updating at each generation the mean of the population (moving the mean of the distribution in the design space). Dependencies between the n variables in the distribution are represented by the scaled covariance matrix.

The **adaptation** of the covariance matrix resembles the approximation of the inverse Hessian matrix in Quasi-Newton methods. The key difference to those methods is that fewer assumptions on the nature of the underlying objective function are made. Neither derivatives nor even the function values are required in the CMA-ES approach. Only a ranking between candidate solutions is exploited to adapt the covariance.

More details are given in Section 4.3, in the context of Optimization Under Uncertainties.

4.2. C-MLMC

As introduced in Section 3, in an optimization problem under uncertainties, we are interested in computing probabilistic loss functions $\mathcal{R}$ and constraints $\mathcal{C}$ of aerodynamic relevant QoI. Each of these QoI, say Q, is associated to the solution u of an aerodynamic problem as $Q = f(u)$. The latter is typically solved using a numerical approximation with a discretization parameter M (number of spatial degrees of freedom); hence Q is approximated by $Q_M = f(u_M)$.

The key idea of Multi Level Monte Carlo (MLMC) [11] is to simultaneously draw Monte Carlo (MC) samples on several approximations Q_{M_l} of Q build on a hierarchy of computational grids with discretization parameters $M_0 < M_1 < ... < M_L = M$ (number of degrees of freedoms).

Considering N_ℓ independent and identically distributed (i.i.d.) realizations $\omega_{i,\ell}$, $i = 1, \cdots, N_\ell$, of the system's random input parameters on each level $0 \leq \ell \leq L$, the MLMC estimator for the mean $\mu = \mathbb{E}[Q]$ of Q is

$$\mu^{\texttt{MLMC}} = \texttt{E}^{\texttt{MC}}\big(Q^0_{N_0,M_0}\big) + \sum_{\ell=1}^{L} \Big(\texttt{E}^{\texttt{MC}}\big(Q^\ell_{N_\ell,M_\ell}\big) - \texttt{E}^{\texttt{MC}}\big(Q^\ell_{N_\ell,M_{\ell-1}}\big) \Big) \ , \tag{10}$$

where $\texttt{E}^{\texttt{MC}}$ denotes the sample average operator and $Q^\ell_{N_\ell,M_\ell}$ is the sample of N_ℓ i.i.d. replications of Q_{M_ℓ}. The same $\omega_{i,\ell}$ are used in both $Q^\ell_{N_\ell,M_\ell}$ and $Q^\ell_{N_\ell,M_{\ell-1}}$.

In [14] we presented an extension of the classical MLMC concept for the estimation of arbitrary order central statistical moments $\mu_p = \mathbb{E}\left[(Q - \mathbb{E}[Q])^p\right]$. The MLMC estimator $\mathtt{m}_p^{\mathtt{MLMC}}$ for arbitrary order p central moment is of the form

$$\mathtt{m}_p^{\mathtt{MLMC}} = h_p\big(Q^0_{N_0,M_0}\big) + \sum_{\ell=1}^{L} \Big(h_p\big(Q^\ell_{N_\ell,M_\ell}\big) - h_p\big(Q^\ell_{N_\ell,M_{\ell-1}}\big)\Big) \ . \tag{11}$$

where h_p denotes an appropriate h-statistic of order p. One of the method's key ingredients is the use of such h-statistics [20] as unbiased central moment estimators with minimal variance for the level-wise contributions.

In [21, 22] we further extended the MLMC concept to accurately approximate the Cumulative distribution function (CDF) of a random system output and robustness measures such as quantiles (also known as Value at Risk, VaR) or coherent risk measures [23] such as the conditional value at risk (CVaR [24]).

Definition 3. ***Quantiles*** *(VaR) are defined as cut-points dividing the range of a probability distribution. The α-quantile q_α is given by:*

$$q^\alpha = VaR^\alpha \equiv \inf\{\vartheta \in \mathbb{R} : F_Q(\vartheta) \geq \alpha\} \qquad \alpha \in (0,1). \tag{12}$$

where $F_Q : \mathbb{R} \to [0,1]$ is the cumulative distribution function (CDF) of a random variable Q.

The Conditional Value at Risk (CVaR) is another well known risk indicator employed in many financial and scientific applications, introduced by Rockafellar [25] as an extension of VaR.

Definition 4. ***CVaR*** *is a risk measure defined as the mean of the so called generalized α-tail distribution:*

$$CVaR^\alpha = \int_{-\infty}^{\infty} z \ dF_Q^\alpha(z), \qquad F_Q^\alpha = \begin{cases} 0, & if \quad z < VaR^\alpha(Q) \\ \frac{F_Q(z)-\alpha}{1-\alpha}, & if \quad z \geq VaR^\alpha(Q) \end{cases} \qquad \alpha \in (0,1). \tag{13}$$

The idea proposed in [21, 22] to approximate simultaneously the CDF, quantiles q^α and $CVaR^\alpha$ of a certain output QoI Q is to first approximate the function $H_Q : \Theta \to \mathbb{R}$ defined as:

$$H_Q(\vartheta) = \mathbb{E}\left(\phi(\vartheta, Q)\right), \qquad \text{with} \qquad \phi(\vartheta, Q) = \vartheta + \frac{1}{1-\tau}(Q-\vartheta)^+ \qquad \text{and} \qquad \tau \in (0,1). \tag{14}$$

This can be done by evaluating $H_Q(\theta_j)$ on a set of points $\theta_j \in \Theta$, $j = 1, \cdot, n$ by a MLMC estimator and then reconstruct an approximate function $\mathtt{P}_{\mathtt{H}}^{\mathtt{MLMC}}(\vartheta) \approx H_Q(\theta)$, $\theta \in \Theta$ by eg. Spline interpolation. Once a MLMC estimator $\mathtt{P}_{\mathtt{H}}^{\mathtt{MLMC}}(\vartheta)$ of $H_Q(\vartheta)$ is accessible, the CDF of Q can be approximated by computing the derivative of $\mathtt{P}_{\mathtt{H}}^{\mathtt{MLMC}}$:

$$F_Q(\vartheta) \approx (1-\tau)\frac{d}{d\vartheta}\mathtt{P}_{\mathtt{H}}^{\mathtt{MLMC}}(\vartheta) + \tau, \tag{15}$$

the τ-quantile (VaR) q^τ (if it exists and is unique) is available via minimization of $\mathtt{P}_{\mathtt{H}}^{\mathtt{MLMC}}(\vartheta)$:

$$q^\tau := \arg\min_{\vartheta \in \mathbb{R}} H_Q(\vartheta) \approx \arg\min_{\vartheta \in \Theta} \mathtt{P}_{\mathtt{H}}^{\mathtt{MLMC}}(\vartheta) \tag{16}$$

and $CVaR^\tau$ can be computed as (see [25])

$$CVaR^\tau := \min_{\vartheta \in \mathbb{R}} H_Q(\vartheta) \approx \min_{\theta \in \Theta} \mathtt{P}_{\mathtt{H}}^{\mathtt{MLMC}}(\vartheta). \tag{17}$$

Details on how to tune the MLMC estimator to obtain simultaneously accurate evaluations of F_Q, q^τ, $CVaR^\tau$ are given in [21].

As underlined and extensively studied in [12], the Continuation-MLMC (C-MLMC) methodology is an extension of the classical MLMC approach that estimates, through a Bayesian update procedure, the optimal number of levels and simulations per level required to achieve a prescribed tolerance. The flexibility and self-tuning nature of the C-MLMC allow us to compute in an effective and robust way statistical moments, CDF, CVaR, VaR of different QoI in a completely automated way for all the candidate designs in the optimization loop.

4.3. Practical aspects: Evolution meets C-MLMC

In a classical CMA-ES methodology, the deterministic objective function $\mathcal{D} : \mathbb{R}^n \to \mathbb{R}$ is computed by solving the underlying deterministic problem with parameters prescribed by χ_k. By combining the CMA-ES and our implementation of C-MLMC we are now able to optimally control the cost required to compute each individual's robust loss function, up to a prescribed tolerance, in the population of candidate solutions, and guarantee a prescribed tolerance on the statistics of the QoIs that are required to compute the robust/reliable loss functions $\mathcal{R} : \mathbb{R}^n \to \mathbb{R}$ and constraints $C_i : \mathbb{R}^m \to \mathbb{R}$.

4.3.1. Sorting

At each generation i, once we have performed a C-MLMC simulation for each design $\chi_k^{(i)}$, we sort the candidate solutions according to their robust/reliable loss function:

$$\mathcal{R}\left(\chi_{\pi(l)}^{(i)}\right) \leq \mathcal{R}\left(\chi_{\pi(k)}^{(i)}\right) \qquad l \leq k \tag{18}$$

where $\pi(\cdot)$ is the permutation of $\{1, \ldots, \lambda\}$ providing the ordering.

4.3.2. Selection and Recombination

In order to update the mean of the population for the next generation, we follow the procedure of Hansen [26]. The new mean is simply the weighted average of the best $\xi < \lambda$ candidates:

$$m^{(i+1)} = \sum_{k=1}^{\xi} w_k \chi_{\pi(k)}^{(i)} = m_i + \sum_{k=1}^{\xi} w_k (\chi_{\pi(k)}^{(i)} - m_i), \qquad \sum_{k=1}^{\xi} w_k = 1 \tag{19}$$

where w_k, $k = 1, \ldots, \xi \in \mathbb{R}_{>0}$ are positive weights. In our implementation we choose $w_k = \frac{1}{\xi}$ and $\xi = \frac{1}{4}\lambda$ to avoid extremely fast convergence of the algorithm towards a local minimum. Several alternatives for the weights and the best number of candidate solutions considered to update the mean are available depending on the complexity and dimensionality of the problem [26].

4.3.3. Adaptation of the covariance

In order to introduce the concept of covariance adaptation, let us consider the population of λ candidates at generation $i+1$ and the following unbiased estimator for the covariance matrix $\hat{C}_\lambda^{(i+1)} = \left(\sigma^{(i)}\right)^2 C^{(i)}$:

$$\hat{C}_\lambda^{(i+1)} = \frac{1}{\lambda} \sum_{k=1}^{\lambda} \left(\chi_k^{(i+1)} - m^{(i)}\right) \left(\chi_k^{(i+1)} - m^{(i)}\right)^T \tag{20}$$

where T denotes the transpose.

Following the same *weighted selection* argument used for the mean in (19), we can define a covariance estimator based only on the best ξ individuals as:

$$\hat{C}_\xi^{(i+1)} = \sum_{k=1}^{\xi} w_k \left(\chi_{\pi(k)}^{(i+1)} - m^{(i)}\right) \left(\chi_{\pi(k)}^{(i+1)} - m^{(i)}\right)^T. \tag{21}$$

The key difference between (20) and (21) is that the former estimates the covariance between the so called *sampled steps* $\chi_k^{(i+1)} - m^{(i)}$ in the population, while the latter just consider the best (successful) ξ selected steps. Hence, sampling from $C_\xi^{(i+1)}$ at the next generation will promote the reproduction of successful steps.

To achieve an effective adaptation of the covariance, information from previous generations should be included. Indeed, after a sufficient number of generations, the scaled covariance matrix could be estimated as an average over all generations of the estimates $\hat{C}^{(i+1)}/(\sigma^{(i)})^2$:

$$C^{(i+1)} = \frac{1}{i+1} \sum_{j=0}^{i} \frac{1}{(\sigma^{(j)})^2} \hat{C}_\xi^{(j+1)} \tag{22}$$

where the variance $\sigma^{(j)}$ has been included in order to make the covariances of different generations comparable. In (22), all generation steps have the same weight. To assign higher weight to the most recent generations an exponential smoothing and an appropriate *learning rate* $0 < c_\xi \leq 1$ are introduced:

$$\begin{aligned} C^{(i+1)} &= (1 - c_\xi) C^{(i)} + c_\xi \frac{1}{(\sigma^{(i)})^2} C_\xi^{(i+1)} \\ &= (1 - c_\xi) C^{(i)} + c_\xi \sum_{k=1}^{\xi} w_k y_{\pi(k)}^{(i+1)} y_{\pi(k)}^{(i+1)T} \end{aligned} \tag{23}$$

and $y_{\pi(k)}^{(i+1)}$ reads as follow:

$$y_{\pi(k)}^{(i+1)} = \frac{\chi_{\pi(k)}^{(i+1)} - m^{(i)}}{\sigma^{(i)}} \tag{24}$$

In our simulation we choose the learning rate for updating the covariance matrix as $c_\xi = \frac{\xi}{4}$. The covariance matrix update in (23) is called rank-ξ-update as the sum of outer products is of rank $\min(\xi, n)$ with probability one [27].

4.3.4. Step size control

The last step required in order to make the C-MLMC CMA-ES algorithm effective is the control of the step-size $\sigma^{(i)}$ (that appears in (24)), in other words the *scale* of the distribution. In addition to the previously presented adaptation rule, Hansen proposed an approach to control the step size based on the concept of cumulative step-size control, or cumulative step length adaptation (CSA). The interested reader may consult [26] for further details. Practically, the step-size is updated as:

$$\sigma^{(i+1)} = \sigma^{(i)} \exp\left(\frac{c_\sigma}{d_\sigma} \left(\frac{\left\| p_\sigma^{(i+1)} \right\|}{\alpha(n)} - 1 \right) \right) \tag{25}$$

where $\alpha(n) = \mathbb{E}\,\|z\|$ with $z \sim \mathcal{N}(0, I)$, $d_\sigma \approx 1$ is a damping parameter used to scale the change in magnitude of $\sigma^{(i)}$ and $p_\sigma \in \mathbb{R}^n$ is called evolution path and denotes a sequence of successive steps over a number of generations:

$$p_\sigma^{(i+1)} = (1 - c_\sigma) p_\sigma^{(i)} + \sqrt{c_\sigma (2 - c_\sigma) \frac{\lambda}{4}} \left(C^{(i)} \right)^{-1/2} \frac{m^{(i+1)} - m^{(i)}}{\sigma^{(i)}}. \tag{26}$$

Finally, c_σ is a backward time horizon of the evolution path that we choose to be equal to $\sqrt{n}$

4.4. C-MLMC CMA-ES Algorithm

In the following Algorithm 1 we denote with i_{max} the maximum number of iterations (generations) of the algorithm, $\boldsymbol{\epsilon}$ a vector of size i_{max} that defines how the tolerance of the C-MLMC algorithm should be reduced during the optimization loop.

As stopping criteria we look at the improvement (in the loss function) of the best designs at each generation of the algorithm. If the performances do not improve by a specified threshold for few generations, we assume that we reached a possibly global optimum and terminate the simulation.

The same strategy and updates presented above can be effectively applied and extended to tackle multi objective optimization problems. However, a multi-objective selection approach should be introduced at the sorting and selection step of the algorithm. We follow the approach of Igel [28] and apply a non-dominated sorting methodology based on the crowding-distance.

Algorithm 1: C-MLMC CMA-ES for Robust Optimization.

CMA-ES$(\lambda,\ \sigma_0,\ m_0,\ i_{MAX},\ \boldsymbol{\epsilon})$
- **Initialize**$(i=0,\ C_i=I,\ m_i=m_0\ \sigma_i=\sigma_0)$
- **while** *(Stop-criteria* **NOT** *reached)* **AND** $i < i_{MAX}$ **do**
  - **for** $k=1,\dots,\lambda$ **do**
    - $\chi_k \sim \mathcal{N}(m_i, \sigma_i^2 C_i)$
    - $\varepsilon_i = \boldsymbol{\epsilon}[i]$
    - **C-MLMC**$(\mathbf{Q}_r^q,\ \mathbf{Q}_c^m,\ \varepsilon_i,\ \chi_k)$
      - **return** $\mathcal{R}\left[\mathbf{Q}_r^q(\widetilde{\chi_k}(\chi_k,\omega),p(\omega))\right],\ \mathcal{C}_j\left[\mathbf{Q}_c^m(\widetilde{\chi_k}(\chi_k,\omega),p(\omega))\right] \quad j=1,\cdots,s$
  - **Sort**: best ξ candidates out of λ according to $\mathcal{R}$ (18)
  - **Mean** m **update** based on ξ candidates using (19)
  - **Step-size** σ **update**: using (25)
  - **Covariance** C **update** using (23)
  - **Generation:** $i = i+1$
- **return** ξ candidates

5. Application to Single-Objective Optimization Under Uncertainties

The above presented methodology is now applied to single objective optimization of the RAE-2822 airfoil under operating and geometric uncertainties. We first introduce the MLMC grid hierarchy and deterministic solver employed to compute the performances of the airfoil. Afterwards, we present the single objective optimization problems under uncertainties (solved with different robust/reliable objective functions) and we compare the results with the solution of the corresponding deterministic optimization problems.

MLMC Grid Hierarchy and Deterministic Solver. In this section we employ a 5-levels structured grid hierarchy for the C-MLMC simulations. The features of the grid levels are presented in Table 4 along with the average computational time required to compute one deterministic simulation using the MSES collection of programs for the analysis of airfoils [29]. MSES solves the steady Euler equations with a finite volume discretization over a streamline grid and is coupled, via the displacement thickness, with a two-equation integral solver for the viscous regions of the boundary layer and trailing wakes.

LEVEL	**Airfoil nodes**	**Cells**	$CTime[s]$
$L0$	47	1739	1.9
$L1$	71	2627	3.2
$L2$	107	3959	5.7
$L3$	161	5957	7.5
$L4$	243	8991	14.7

Table 4: MLMC 5-levels grid hierarchy for the RAE2822 problem.

5.1. Maximization of Lift-Drag Ratio

Deterministic Single Point Maximization of Lift-Drag ratio at fixed Mach and AoA: SO-DO1. An interesting problem that arises during the preliminary stage of the design process is the maximization of the lift-drag ratio L/D of the airfoil for a specific combination of angle of attack and Mach number. We can particularize the SO-DO in (1) for a specific cruise Mach number condition M_∞ and angle of attack α_∞ (see Table 5 column "reference") and define the following single point deterministic shape optimization problem:

$$\text{SO-DO1}: \max_{\chi \in X} \quad L/D^{(M_\infty,\alpha_\infty)}(x,p) \tag{27}$$

In the feasible design space X, we constrain the shape of the airfoil by requiring enough space for the fuel/torque box (see Figure 3) and the final are to be at least 75% of the original section of the RAE-2822.

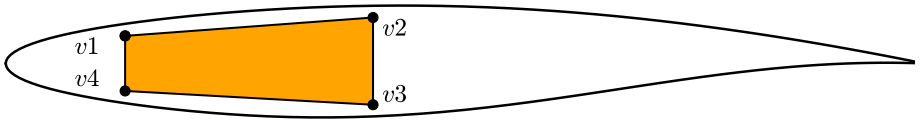

Figure 3: Geometrical trapezoid box constraint.

The coordinates of the box vertexes are: $v1 = (0.13, 0.03)$, $v2 = (0.4, 0.05)$, $v3 = (0.4, -0.045)$, $v4 = (0.13, -0.03)$. This is a reasonable requirement to build an aircraft wing with an appropriate inner volume to accommodate the fuel tank and a torque box. Additionally such requirement naturally rejects, from the population of candidate individuals, all degenerate airfoil sections.

The design parameters χ are the PARSEC coefficients (see Section 3.1.1 for definition), which are constrained to the ranges in Table 6, column "Design range".

Robust Single Objective Maximization of Lift-Drag ratio: SO-RDO1. Instead of solving the optimization problem for a single combination of Mach number and angle of attack, as in SO-DO1 (see (27)), we now consider the problem of robustly optimize the shape of the RAE-2822 airfoil affected by operating uncertainties (system parameters: $p(\omega)$, Mach number and angle of attack in Table 5) and geometric uncertainties (PARSEC parameters in Table 6) at the same time. The operating uncertainties considered in this problem are representative of mild atmospheric gust that an aircraft may encounter during cruise. The geometric uncertainties, on the other hand, are representative of manufacturing tolerances.

All uncertain parameters are modeled as truncated normal distributions that we denote by $\mathcal{TN}(\mu, \sigma, a, b)$, where μ is the location or mean, σ is the standard deviation, a is the minimum allowed value and b is the maximum one (in percent with respect to the mean).

	Quantity	**Reference** (r)	**Uncertainty**
Operating parameters	α_∞	2.31	$\mathcal{TN}(r, 2\%r, -2\%r, +2\%r)$
	M_∞	0.730	$\mathcal{TN}(r, 2\%r, -2\%r, +2\%r)$
	Re_c	$6.5 \cdot 10^6$	–
	$p_\infty\ [Pa]$	101325	–
	$T_\infty\ [K]$	288.5	–

Table 5: Operating parameters and uncertainties for the RAE2822 problem.

The design parameters χ are the PARSEC parameters in Table 6. In the actual stage of the airfoil, uncertainty is added to those parameters so that $\widetilde{\chi}(\chi, \omega) = \chi + \delta\chi(\omega)$ with $\delta\chi(\omega)$ as in Table 6 column "Uncertainty".

Instead of using a deterministic loss function, as in SO-DO1, we consider here a robust loss function defined as the difference of the mean and the standard deviation of the lift-drag ratio L/D of the airfoil.

$$\text{SO-RDO1} : \max_{x \in X} \ \mathcal{R}\left[L/D(\widetilde{\chi}(\chi, \omega), p(\omega))\right] = \mu_{L/D}(\widetilde{\chi}(\chi, \omega), p(\omega)) - \sigma_{L/D}(\widetilde{\chi}(\chi, \omega), p(\omega)) \tag{28}$$

In the feasible design space we constraint, as in the deterministic problem SO-DO1, the shape of the airfoil by requiring enough space for the fuel/torque box (see Figure 3) and the final shape to be at lease 75% of the original section of the RAE-2822. It is worth underline that the geometrical constraint is enforced only on the nominal shape χ, not on the perturbed one $\widetilde{\chi}$.

	Quantity	PARSEC(r)	Uncertainty	Design range
Geometric parameters	R_s	0.00839	$\mathcal{TN}(r, 1\%r, -1\%r, +1\%r)$	$[70\%r,\ 130\%r]$
	R_p	0.00853	$\mathcal{TN}(r, 1\%r, -1\%r, +1\%r)$	$[70\%r,\ 130\%r]$
	x_s	0.431	$\mathcal{TN}(r, 1\%r, -2\%r, +2\%r)$	$[50\%r,\ 150\%r]$
	x_p	0.346	$\mathcal{TN}(r, 1\%r, -2\%r, +2\%r)$	$[50\%r,\ 150\%r]$
	y_s	0.063	$\mathcal{TN}(r, 1\%r, -2\%r, +2\%r)$	$[70\%r,\ 130\%r]$
	y_p	-0.058	$\mathcal{TN}(r, 1\%r, -2\%r, +2\%r)$	$[70\%r,\ 130\%r]$
	C_s	-0.432	$\mathcal{TN}(r, 1\%r, -1\%r, +1\%r)$	$[50\%r,\ 150\%r]$
	C_p	0.699	$\mathcal{TN}(r, 1\%r, -1\%r, +1\%r)$	$[50\%r,\ 150\%r]$
	θ_s	-11.607	—	—
	θ_p	-2.227	—	—

Table 6: PARSEC parameters of the RAE2822 airfoil, geometric uncertainties applied on the shape, and design range for the geometric parameters.

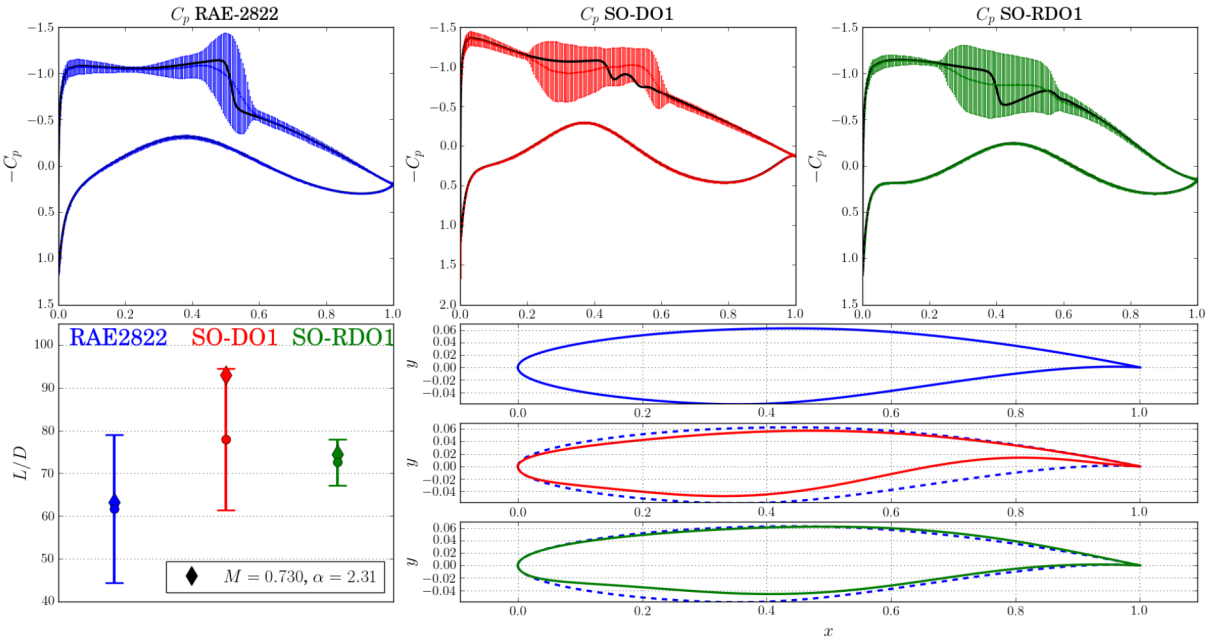

Figure 4: Performances of the SO-RDO1 and SO-DO1 airfoil compared with the original RAE-2822. The upper plots present the uncertain C_p profile of the airfoils under operating and geometric uncertainties. The lower left plot presents the L/D variation (mean $\pm$ two standard deviations). The diamond symbol represents the performance of the airfoil at design condition (airfoil operating at $M_\infty = 0.730,\ \alpha_\infty = 2.31$).

Comparison of Optimized Shapes. In Figure 4 and Table 7 we present the results of the robust (SO-RDO1) and deterministic (SO-DO1) optimization of the L/D ratio. We can observe that the deterministically optimized airfoil is able to achieve the best performance at design condition, however the L/D ratio is highly sensitive to small variations of the geometry and operating conditions.

The robust airfoil SO-RDO1 is equipped with a relatively large leading edge and much wider pressure side trailing edge angle. The quasi constant pressure plateau and the large aft chamber, compared to the SO-DO1, are capable to reduce the L/D dispersion.

	RAE2822	SO-DO1	SO-RDO1
$M = 0.729$ $\alpha = 2.31$ Fixed Geom.	$L/D = 63.2$	$\mathbf{L/D = 92.8}$	$L/D = 74.5$
$M = \mathcal{TN}(r, 2\%, -2\%, +2\%)$ $\alpha = \mathcal{TN}(r, 2\%, -2\%, +2\%)$ Uncertain Geom.	$L/D = 61.7$ ± 8.6 (14%)	$L/D = \mathbf{77.9}$ ± 8.2 (10.5%)	$L/D = 72.9$ $\pm \mathbf{2.6}$ (**3.5**%)

Table 7: Performances and variabilities (mean ± two standard deviations) of the SO-DO1 and SO-RDO1 airfoil compared with the original RAE-2822 at design conditions and when they operate in an uncertain environment.

5.2. Minimization of Drag Coefficient

In a later stage of the design process, when structural considerations are introduced and the aircraft mission is appropriately defined, we might have tighter geometrical constraints and we are required to match a specific cruise lift condition.

Deterministic Single Point Minimization of Drag at fixed Mach and Lift: SO-DO2 (SP). We can particularize SO-DO problem (1) for a specific cruise Mach number condition M_∞ and lift coefficient C_L^* and define the following single point deterministic shape optimization problem:

$$\text{SO-DO2 (SP)} : \min_{\chi \in X} \quad C_D^{(M_\infty, C_L^*)}(\chi, p) \tag{29}$$

It is worth underline that in order to enforce the C_L^* constraint on each design candidate, we compute for each of them a converged solution with an initial angle of attach α which we then gradually increase/decrease in order to match the prescribed lift coefficient.

Also for this problem, the design parameters χ are the PARSEC coefficients (see Section 3.1.1 for definition), constrained in the ranges indicated in Table 8. The constraints in X are now imposed on the thickness of the airfoil in order to attain a shape capable of matching the required structural requirements. In our simulations we set the thickness of the airfoil (PARSEC parameters y_s and y_p) to match exactly that of the original RAE-2822 airfoil (see Figure 5 for comparison of optimal and initial reference RAE2822 airfoil).

	Quantity	PARSEC - RAE-2822(r)	Design range
Geometric parameters	R_s	0.00839	$[70\%r,\ 130\%r]$
	R_p	0.00853	$[70\%r,\ 130\%r]$
	x_s	0.431	$[50\%r,\ 150\%r]$
	x_p	0.346	$[50\%r,\ 150\%r]$
	y_s	0.063	–
	y_p	-0.058	–
	C_s	-0.432	$[50\%r,\ 150\%r]$
	C_p	0.699	$[50\%r,\ 150\%r]$
	θ_s	-11.607	$[50\%r,\ 150\%r]$
	θ_p	-2.227	$[50\%r,\ 150\%r]$

Table 8: PARSEC parameters of the RAE2822 airfoil and feasible design space range for the geometric parameters.

As presented in [30], such optimization problems generally lead to airfoil shapes that are optimal only in a narrow range of Mach numbers (leading to so called *localized optimization*). The optimal shape will generally be shock-less and/or will present a bump in a specific location in order to fill the transitional separation bubble to reduce the drag in the specific cruise condition. The performance of such shapes degrades quite fast away form the design conditions as the bump location and the curvature of the airfoil are not able to

avoid the shock and/or fill the separation bubble for other combinations of Mach number and lift coefficient. Additionally if the geometry of the airfoil is affected by uncertainties due to manufacturing tolerances and/or temporary factors such as icing or aeroelastic deformation of the wing, the shape can be ineffective even in the prescribed design conditions.

Figure 5 presents the results of single point optimization of the RAE 2822 airfoil for different cruise Mach number ($M = 0.7, 0.725, 0.75, 0.775, 0.8$) and fixed $C_L^* = 0.5$. As it is clear form the figure, the performance (drag) degrades quite fast away from design conditions.

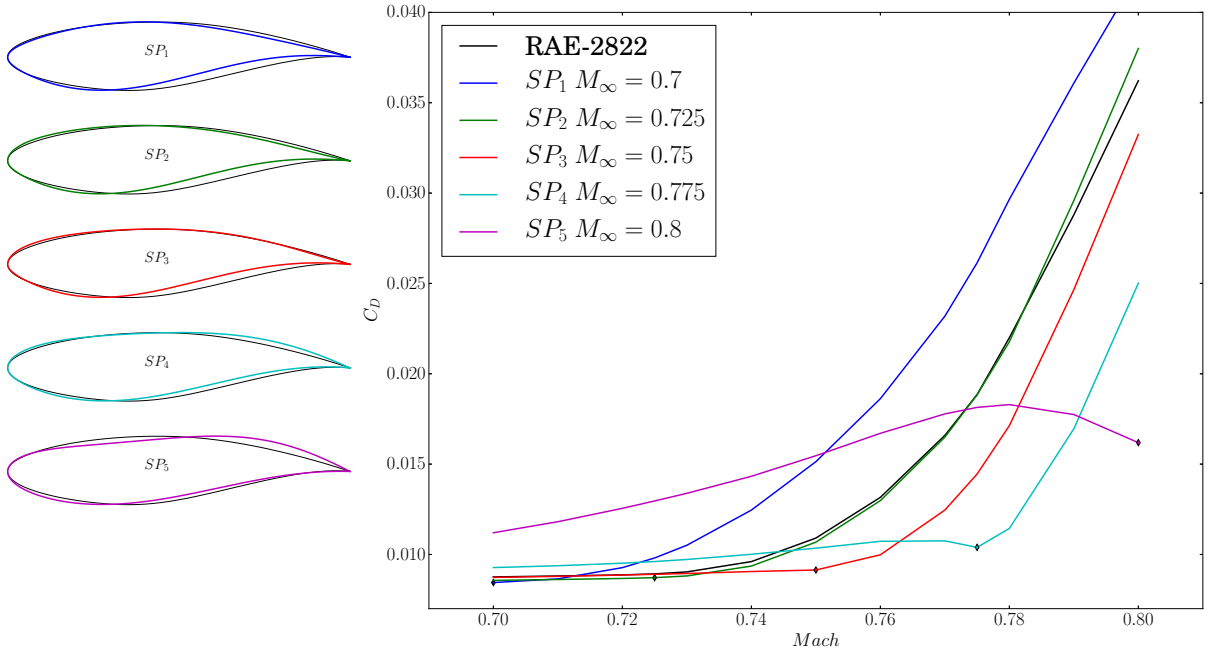

Figure 5: Single Point optimization of the RAE 2822 airfoil for different cruise Mach number and fixed $C_L^* = 0.5$. The thickness of the airfoils is constrained to be the same as the original RAE 2822 airfoil, while the other PARSEC geometrical parameters are free.

Multi Point Minimization of Drag at fixed Lift: SO-DO2 (MP). An intuitive approach to improve off-design performances of transonic airfoils, generally denoted as multi-point optimization, is based on a trade off between different design conditions [31] [32].

Instead of optimizing an objective function for a single discrete flight condition as in SP-DO2 (29), we consider a weighted linear combination of m flight conditions:

$$\text{SO-DO2 (MP)} : \min_{\chi \in X} \quad \sum_{i=1}^{m} w_i \cdot C_D^{(M_\infty^i, C_L^*)}(\chi, p) \tag{30}$$

The number of m flight conditions, the choice of M_∞^i and the weights w_i are determined by the designer in order to fulfill specific performance or mission requirements (no sound theoretical principles are available for these choices). Empirical sophisticated ways of choosing multi point flight conditions and their weights can be found in [33].

In this analysis we choose two, three and five equally weighted flight conditions between $M_\infty = 0.7$ and 0.8 for the design denoted by MP_2^U, MP_3^U, MP_5^U respectively in Figure 6. Additionally we also consider three and five flight conditions weighted using the area underlying a symmetric beta distribution centered in $M_\infty = 0.75$ ($\mathcal{B}(2, 2, 0.1, M_\infty - 0.05)$) for the designs MP_3^β, MP_5^β (see Table 9). Figure 6 presents the results of the multi point shape optimization of the RAE 2822 airfoil for different cruise Mach numbers

$(M = 0.7, 0.725, 0.75, 0.775, 0.8)$ and fixed $C_L^* = 0.5$. A critical discussion is postponed to the next section where these results are also compared to those obtained in the OUU case.

MP Design	**Flight conditions** (M_∞^i)	**Weights** (w_i)
MP_2^U	0.7, 0.8	0.5, 0.5
MP_3^U	0.7, 0.75, 0.8	1/3, 1/3, 1/3
MP_3^β	0.7, 0.75, 0.8	0.15625, 0.6875, 0.15625
MP_5^U	0.7, 0.725, 0.75, 0.775, 0.8	1/5, 1/5, 1/5, 1/5, 1/5
MP_5^β	0.7, 0.725, 0.75, 0.775, 0.8	0.04296875, 0.2734375, 0.3671875, 0.2734375, 0.04296875

Table 9: Flight conditions and weight for deterministic multi point optimization.

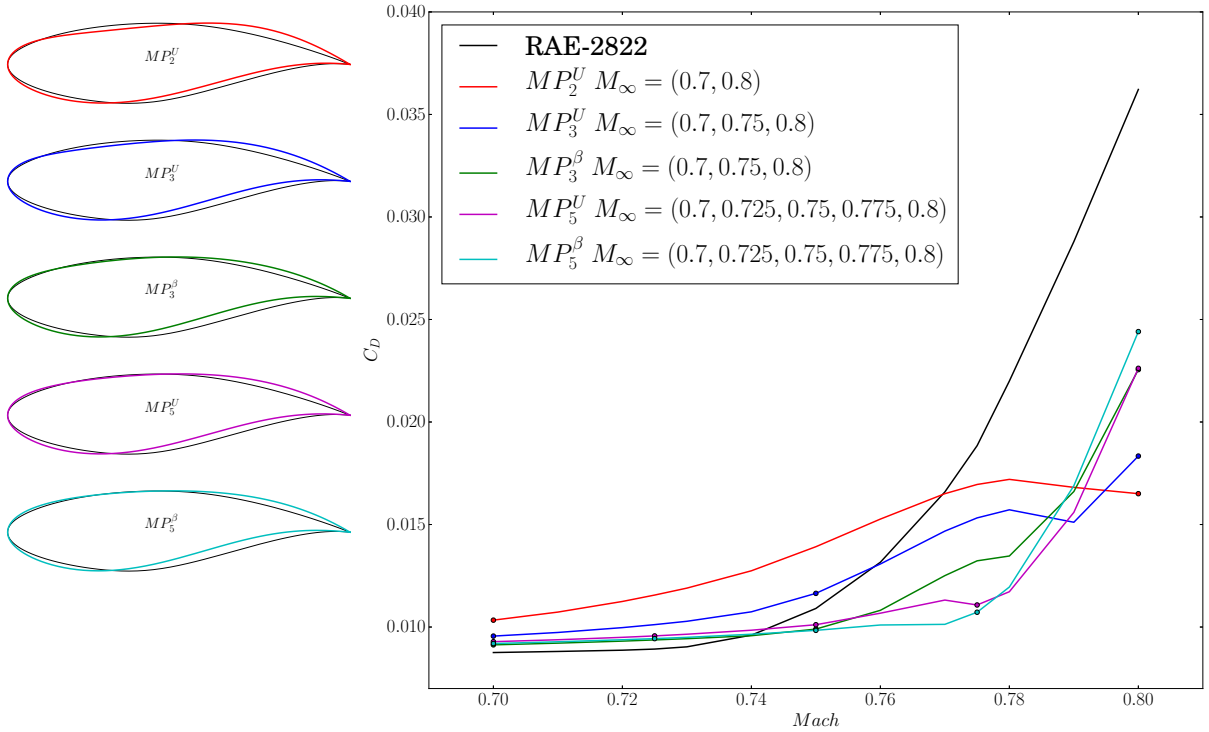

Figure 6: Multi Point optimization of the RAE 2822 airfoil for different choices of cruise Mach number and weights (fixed $C_L^* = 0.5$). The diamonds on each C_D-Mach curve indicate the design condition. The thickness of the airfoils is constrained to be the same as the original RAE 2822 airfoil, while the other PARSEC geometrical parameters are free.

Robust and Reliable Single Objective Minimization of Drag at fixed Lift: SO-RDO2. Instead of solving the optimization problem for a prescribed Mach number, as in SO-DO2 (29), or a weighted sum of flight conditions, as in SO-DO2 (MP) (30), we now consider the problem of optimizing the shape of the RAE-2822 airfoil affected by uncertainties using different robust and reliable loss functions.

The operating uncertainty, namely the Mach number, is modeled as a beta distribution denoted by $\mathcal{B}(a, b, s, loc)$, where a and b are the distribution parameters. As the beta distribution is defined on the $[0, 1]$ interval, the parameters s and loc are used to scale and shift the distribution's support, respectively (see Table 10).

The operating uncertainty considered in this problem is representative of atmospheric fluctuations during a flight mission. The design parameters are the PARSEC parameters; their nominal values and design range

	Quantity	Reference (r)	Uncertainty
Operating parameters	C_L	0.5	–
	M_∞	0.75	$\mathcal{B}(2, 2, 0.1, M_\infty - 0.05)$
	Re_c	$6.5 \cdot 10^6$	–
	$p_\infty\ [Pa]$	101325	–
	$T_\infty\ [K]$	288.5	–

Table 10: Operating parameters and uncertainties for the RAE2822 problem.

are reported in Table 8. No geometrical uncertainties are considered in this case.

In order to compare the advantages and effectiveness of different probabilistic loss functions we consider here the following robust optimization problem:

$$\text{SO-RDO2}: \begin{cases} \min\limits_{\chi \in X} & \mathcal{R}\left[C_D(\chi, p(\omega))\right] \\ s.t & C_L(\chi, p(\omega)) = C_L^* \end{cases} \tag{31}$$

and consider the loss functions presented in Table 11.

$\mathcal{R}_\mu\left[C_D\right]$	$\mu_{C_D}(\chi, p(\omega))$
$\mathcal{R}_{\mu,\sigma}\left[C_D\right]$	$\mu_{C_D}(\chi, p(\omega)) + \sigma_{C_D}(\chi, p(\omega))$
$\mathcal{R}_{\mu,\sigma,\gamma}\left[C_D\right]$	$\mu_{C_D}(\chi, p(\omega)) + \sigma_{C_D}(\chi, p(\omega)) + (\mu_{C_D}(\chi, p(\omega)) \cdot \gamma_{C_D}(\chi, p(\omega))$
$\mathcal{R}_{VaR^{90}}\left[C_D\right]$	$VaR^{90}_{C_D}(\chi, p(\omega))$
$\mathcal{R}_{CVaR^{90}}\left[C_D\right]$	$CVaR^{90}_{C_D}(\chi, p(\omega))$

Table 11: Probabilistic loss functions for problem SO-RDO2.

Comparison of Optimized Shapes. In Figure 7 we show the pressure coefficient and the deterministic optimized shapes (SP and MP) and robust/reliable obtained shapes with different probabilistic loss functions (Table 11) under operating uncertainties presented in Table 10.

The first observation we can draw from Figure 7 is that MP designs are able to effectively reduce the variability in the pressure coefficient compared to SP designs. Indeed, we can observe, in particular for M_5^U and M_5^β, quasi constant pressure plateau on the suction side of the airfoils, capable of reducing the intensity of the shock wave. The geometries of M_5^U and M_5^β are characterized by relatively large leading edge radius, low curvature suction side and an increased aft chamber. The pressure profile and the geometry of the airfoil obtained by minimizing just the expectation of drag coefficient $\mathcal{R}_\mu\left[C_D\right]$ appear very similar to M_5^β. This is indeed justified by the choice of weights in M_5^β that mimic an empirical mean over five flight conditions. On the other hand the airfoils obtained by minimizing 90% CVaR of C_D, $\mathcal{R}_{CVaR^{90}}\left[C_D\right]$, as well as those obtained by minimizing the first three statistical moments $\mathcal{R}_{\mu,\sigma,\gamma}\left[C_D\right]$ seem to promote the development of the shock in the front part of the airfoil in order to reduce the variability in the aft part of it.

In order to effectively analyze the performances of the deterministic and robust/reliable optimized shapes in the uncertain environment, we present in Figure 8 the Cumulative Distribution Function (CDF) of the drag coefficient C_D computed using the MLMC methodology. We observe, as underlined above for the C_p, that MP designs are able to reduce the variability in the drag coefficient compared to SP designs. The airfoil obtained by minimizing the first three statistical moments $\mathcal{R}_{\mu,\sigma,\gamma}\left[C_D\right]$ presents an heavy tail on the side of low drag and seems the most reliable candidate. The airfoil obtained with 90% VaR minimization, $\mathcal{R}_{VaR^{90}}\left[C_D\right]$ is indeed the candidate that have the lowest 90%-quantile C_D but presents an heavy tail on the side of high drag. On the other hand, the airfoil obtained with 90% CVaR minimization, $\mathcal{R}_{CVaR^{90}}\left[C_D\right]$ is able to effectively control the tail of the distribution at the price of a higher mean value of C_D.

6. Application to Multi-Objective Optimization Under Uncertainties

In this section, the above presented methodology is applied to multi objective optimization under uncertainties of the RAE-2822 airfoil.

6.1. Optimization of Lift and Drag

Multi Objective Deterministic Optimization of Lift and Drag: MO-DO1. We now consider two competing objectives to be optimized simultaneously, namely minimize the drag coefficient C_D and maximize the lift coefficient C_L for a specific combination of Mach number and angle of attack:

$$\text{MO-DO1} : \underset{\chi \in X}{\text{P-min}} \;\; \{C_D^{(M_\infty, \alpha_\infty)}(x, p), -C_L^{(M_\infty, \alpha_\infty)}(\chi, p)\} \tag{32}$$

We use as design variables χ the vertical position of 15 nodes Free Form Deformation (FFD) box (Figure 2 and definition in Section 3.1.2). The FFD box has the same length of the airfoil and the thickness of the box is 25% of the airfoil chord. The design range for the nodes of the FFD box is 10% of the airfoil chord in vertical direction, while is fixed in horizontal direction.

Multi Objective Robust Design Optimization of Lift and Drag with Operating Uncertainties: MO-RDO1. We now consider two competing robust objectives to be optimized simultaneously, namely minimize the drag coefficient C_D and its dispersion and maximise the lift coefficient and reduce its dispersion. We consider, first, only operating uncertainties as in Table 5 affecting the flow surrounding the airfoil and we use as design variables χ the Free Form Deformation (FFD) box coefficients (Figure 2).

$$\text{MO-RDO1} : \underset{\chi \in X}{\text{P-min}} \;\; \{\mathcal{R}_D\left[C_D(\chi, p(\omega))\right], \mathcal{R}_L\left[C_L(\chi, p(\omega))\right]\} \tag{33}$$

with:

$$\begin{aligned} \mathcal{R}_D\left[C_D(\chi, p(\omega))\right] &= \mu_{C_D}(\chi, p(\omega)) + \sigma_{C_D}(\chi, p(\omega)) \\ \mathcal{R}_L\left[C_L(\chi, p(\omega))\right] &= -\mu_{C_L}(\chi, p(\omega)) + \sigma_{C_L}(\chi, p(\omega)) \end{aligned} \tag{34}$$

We consider as uncertain operating parameters those defined for the single objective problem SO-RDO2 (see Table 5)

In Figure 9 we present the results of MO-DO1 and MO-RDO1. For the candidate designs in the deterministic Pareto set (blue points, with lift coefficient higher and drag coefficient lower than the original RAE2822) and the RAE-2822 airfoil (black point) we perform an uncertainty analysis and compute the mean value (red square) and dispersion of the airfoils C_D and C_L (red ellipses correspond to two standard deviations) when they are operated in the uncertain environment. The blue stars represent candidates in the deterministic Pareto set that are very unstable when operating in the uncertain environment. Small variations in the angle of attack and Mach number lead to separated flow on the suction side of such airfoils (no ellipse is drown for those candidates). We perform the same uncertainty analysis also for the candidate design obtained by solving the MO-RDO1 (yellow points in the robust pareto front indicate the value of the robust loss function for C_L and C_D) and compute the mean value (green square) and dispersion (green ellipses).

It is interesting to notice in Figure 9 a gathering of robust optimal candidates and their means around $C_L \approx 0.75$ and $C_D \approx 0.011$. Such robust candidates have quite similar performances and dispersion around the mean.

Multi Objective Robust Design Optimization of Lift and Drag with operating and geometric uncertainties: MO-RDO2. Lastly we consider the multi objective problem of minimizing the drag coefficient C_D and its dispersion and maximizing the lift coefficient and reducing its dispersion under operating uncertainties (system parameters $p(\omega)$, Mach number and angle of attack in Table 5) and geometric uncertainties (PARSEC parameters in Table 6) at the same time. In this set of simulations the design parameters χ, are PARSEC

parameters and in the actual shape of the airfoil, uncertainty is added to those parameters ($\widetilde{\chi} = \chi + \delta\chi(\omega)$ as in Table 6 third column).

$$\text{MO-RDO2} : \underset{\chi \in X}{\text{P-min}} \ \left\{ \mathcal{R}_D \left[C_D(\widetilde{\chi}(\chi,\omega), p(\omega)) \right], \mathcal{R}_L \left[C_L(\widetilde{\chi}(\chi,\omega), p(\omega)) \right] \right\} \tag{35}$$

with:

$$\begin{aligned} \mathcal{R}_D \left[C_D(\widetilde{\chi}(\chi,\omega), p(\omega)) \right] &= \mu_{C_D}(\widetilde{\chi}(\chi,\omega), p(\omega)) + \sigma_{C_D}(\widetilde{\chi}(\chi,\omega), p(\omega)) \\ \mathcal{R}_L \left[C_L(\widetilde{\chi}(\chi,\omega), p(\omega)) \right] &= -\mu_{C_L}(\widetilde{\chi}(\chi,\omega), p(\omega)) + \sigma_{C_L}(\widetilde{\chi}(\chi,\omega), p(\omega)) \end{aligned} \tag{36}$$

We compare the results with MO-DO1 but in this set of simulations we use the PARSEC coefficients as design parameters (see Table 6).

In Figure 10 we present the results of MO-RDO2 and MO-DO1. We perform, as for the previous case, an uncertainty analysis for the deterministic and robust candidates that dominate the original RAE-2822 (with lift coefficient higher and drag coefficient lower) and compute the mean value (red squares for the deterministic optimal and yellow squares for the robust optimal candidates) and dispersion of the airfoils C_D and C_L (red ellipses for the deterministic and green for robust candidates that correspond to two standard deviations) when they are operated in the uncertain environment. The blue stars represent candidates in the deterministic Pareto set that are very unstable when operating in the uncertain environment. Small variations in the geometry, angle of attack or Mach number lead to separated flow on the suction side of such airfoils. We can clearly identify, even better than in the previous case with only operating uncertainties, a much higher stability of the performances of the robust optimized airfoils when operated in an uncertain environment and when affected by geometrical uncertainties.

7. Conclusions

In this work we have presented how the C-MLMC approach can be efficiently integrated in an optimization evolutionary strategy algorithm to perform single and multi objective robust and reliability based design optimization of transonic airfoils affected by a considerable number of operating and geometric uncertainties. We showed how to efficiently compute loss functions and probabilistic constraints that include central statistical moments and risk measures.

We demonstrated with single and multi objective optimization problems that such methodology can be efficiently employed to design transonic airfoils that are less sensitive to uncertainties. We believe that the technique has the potential to be extended to more complex problems where the stability and the reliability of the aerodynamic system is of crucial importance.

Acknowledgments

This research has received funding from the European Union's Seventh Framework Programme for research, technological development and demonstration under grant agreement no ACP3-GA-2013-605036 (Uncertainty Management for Robust Industrial Design in Aeronautics (UMRIDA) project). The first two authors acknowledge also support from the Center for ADvanced MOdeling Science (CADMOS).

Bibliography

[1] Whitcomb, R.T.: Review of nasa supercritical airfoils. ICAS paper (74-10) (1974) 25–30
[2] Lewis, R.M., Huyse, L.: Aerodynamic shape optimization of two-dimensional airfoils under uncertain conditions. Technical report, INSTITUTE FOR COMPUTER APPLICATIONS IN SCIENCE AND ENGINEERING HAMPTON VA (2001)
[3] Li, W., Huyse, L., Padula, S.: Robust airfoil optimization to achieve drag reduction over a range of mach numbers. Structural and Multidisciplinary Optimization **24**(1) (2002) 38–50
[4] Winston, W.L.: Operations research. algorithms and applications (1994)
[5] Tootkaboni, M., Asadpoure, A., Guest, J.K.: Topology optimization of continuum structures under uncertainty–a polynomial chaos approach. Computer Methods in Applied Mechanics and Engineering **201** (2012) 263–275

[6] Dodson, M., Parks, G.T.: Robust aerodynamic design optimization using polynomial chaos. Journal of Aircraft **46**(2) (2009) 635–646
[7] Ho, S., Yang, S.: A fast robust optimization methodology based on polynomial chaos and evolutionary algorithm for inverse problems. IEEE Transactions on Magnetics **48**(2) (2012) 259–262
[8] Sankaran, S., Audet, C., Marsden, A.L.: A method for stochastic constrained optimization using derivative-free surrogate pattern search and collocation. Journal of Computational Physics **229**(12) (2010) 4664–4682
[9] Simpson, T.W., Mauery, T.M., Korte, J.J., Mistree, F.: Kriging models for global approximation in simulation-based multidisciplinary design optimization. AIAA journal **39**(12) (2001) 2233–2241
[10] Heinrich, S.: Monte Carlo complexity of global solution of integral equations. Journal of Complexity **14**(2) (1998) 151–175
[11] Giles, M.B.: Multilevel Monte Carlo path simulation. Operations Research **56**(3) (2008) 607–617
[12] Pisaroni, M., Nobile, F., Leyland, P.: A Continuation Multi Level Monte Carlo (c-mlmc) method for uncertainty quantification in compressible inviscid aerodynamics. Computer Methods in Applied Mechanics and Engineering **326** (2017) 20–50
[13] Collier, N., Haji-Ali, A.L., Nobile, F., von Schwerin, E., Tempone, R.: A continuation Multilevel Monte Carlo algorithm. BIT Numerical Mathematics (2014) 1–34
[14] Pisaroni, M., Krumscheid, S., Nobile, F.: Quantifying uncertain system outputs via the Multilevel Monte Carlo method–Part I: Central moment estimation. Mathicse technical report no. 23.2017, Ecole Polytechnique Fédérale de Lausanne (2017)
[15] Sobieczky, H.: Parametric airfoils and wings. In: Recent Development of Aerodynamic Design Methodologies. Springer (1999) 71–87
[16] Sederberg, T.W., Parry, S.R.: Free-form deformation of solid geometric models. ACM SIGGRAPH computer graphics **20**(4) (1986) 151–160
[17] Perry, E., Balling, R., Landon, M.: A new morphing method for shape optimization. In: Proceedings of 7th AIAA/USAF/NASA/ISSMO Symposium on Multidisciplinary Analysis & Optimization, Saint-Louis, Etats-Unis. Number 2896 (1998)
[18] Yamazaki, W., Mouton, S., Carrier, G.: Efficient design optimization by physics-based direct manipulation free-form deformation. AIAA Paper **5953** (2008) 2008
[19] Hansen, N., Ostermeier, A.: Completely derandomized self-adaptation in evolution strategies. Evolutionary computation **9**(2) (2001) 159–195
[20] Dwyer, P.S.: Moments of any rational integral isobaric sample moment function. Ann. Math. Stat. **8**(1) (1937) 21–65
[21] Krumscheid, S., Nobile, F.: Multilevel Monte Carlo approximation of functions. Mathicse technical report no. 12.2017, Ecole Polytechnique Fédérale de Lausanne (2017)
[22] Pisaroni, M., Krumscheid, S., Nobile, F.: Quantifying uncertain system outputs via the Multilevel Monte Carlo method–Part II: Distribution and robustness measures. in prepartation
[23] Delbaen, F.: Coherent risk measures. Blätter der DGVFM **24**(4) (2000) 733–739
[24] Rockafellar, R.T.: Coherent approaches to risk in optimization under uncertainty. In: OR Tools and Applications: Glimpses of Future Technologies. Informs (2007) 38–61
[25] Rockafellar, R.T., Uryasev, S.: Conditional value-at-risk for general loss distributions. Journal of banking & finance **26**(7) (2002) 1443–1471
[26] Hansen, N.: The cma evolution strategy: A tutorial. arXiv preprint arXiv:1604.00772 (2016)
[27] Hansen, N., Müller, S.D., Koumoutsakos, P.: Reducing the time complexity of the derandomized evolution strategy with covariance matrix adaptation (cma-es). Evolutionary computation **11**(1) (2003) 1–18
[28] Igel, C., Hansen, N., Roth, S.: Covariance matrix adaptation for multi-objective optimization. Evolutionary computation **15**(1) (2007) 1–28
[29] Drela, M.: A user's guide to mses 3.05. Massachusetts Institute of Technology (MIT), Cambridge (2007)
[30] Drela, M.: Pros and cons of airfoil optimization. Frontiers of computational fluid dynamics **1998** (1998)
[31] Campbell, R.L.: Efficient viscous design of realistic aircraft configurations. AIAA paper **2539** (1998) 1998
[32] Elliott, J., Peraire, J.: Constrained, multipoint shape optimisation for complex 3d configurations. The Aeronautical Journal **102**(1017) (1998) 365–376
[33] Lyu, Z., Kenway, G.K., Martins, J.R.: Aerodynamic shape optimization investigations of the common research model wing benchmark. AIAA Journal (2014)

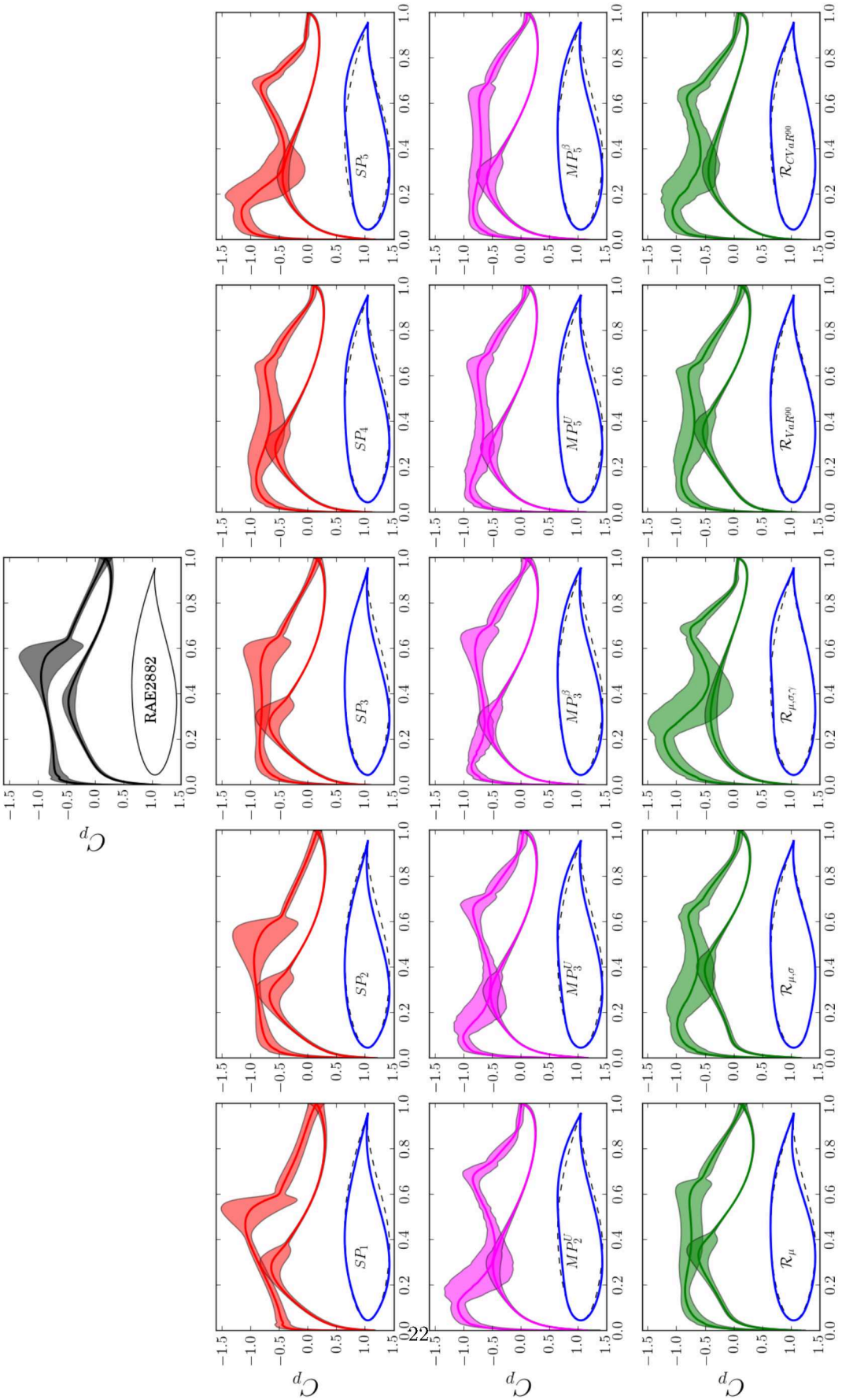

Figure 7: Pressure coefficient C_p (mean $\pm$ two standard deviations) and shape of the RAE 2822 (in black), the deterministic optimized shapes (SP in red and MP in magenta) and robust/reliable shapes obtained with different probabilistic loss functions (in green) under operating uncertainties.

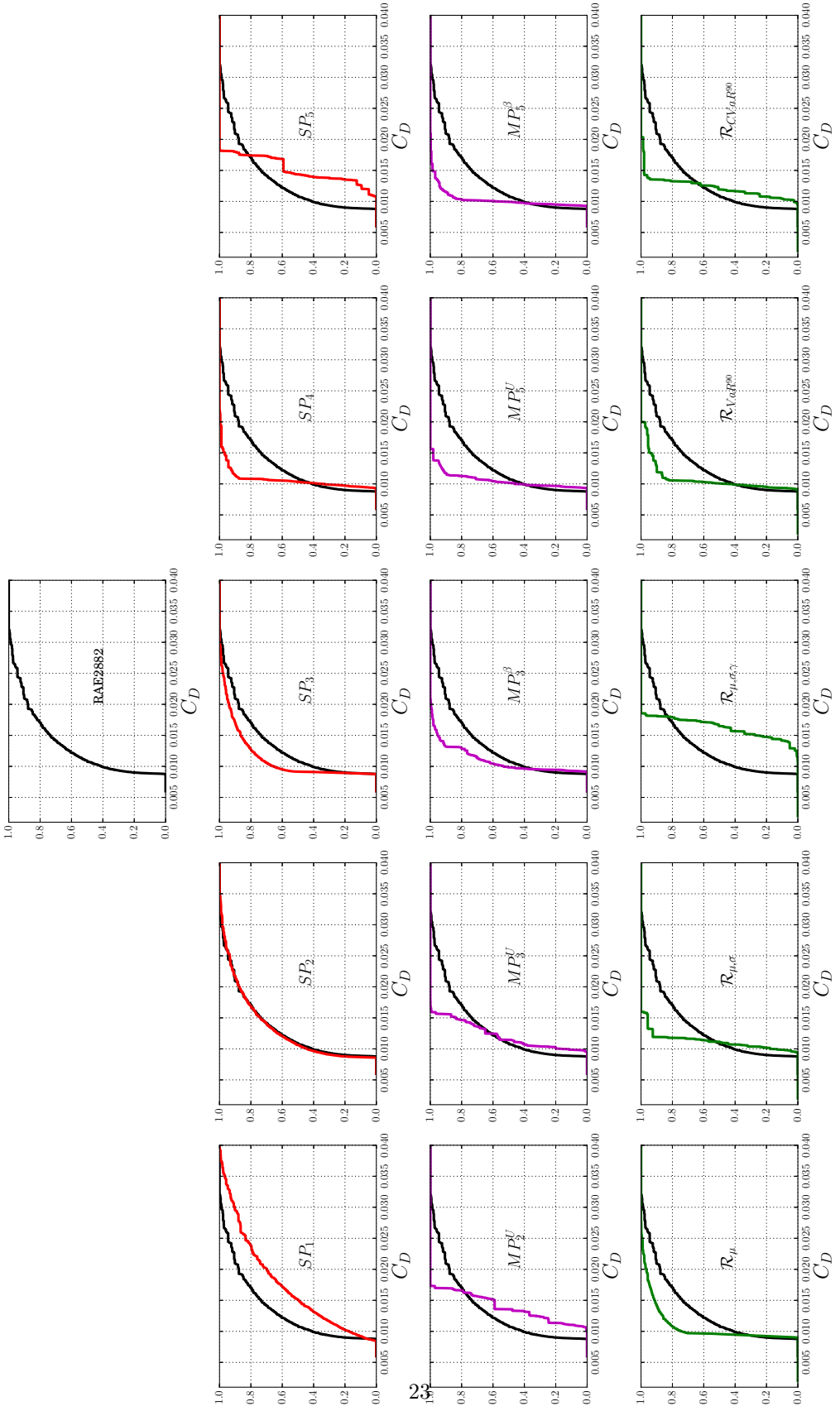

Figure 8: CDF of the drag coefficient C_D of the RAE 2822 (in black), the deterministic optimized shapes (SP in red and MP in magenta) and robust/reliable shape obtained with different probabilistic loss functions (in green) under operating uncertainties.

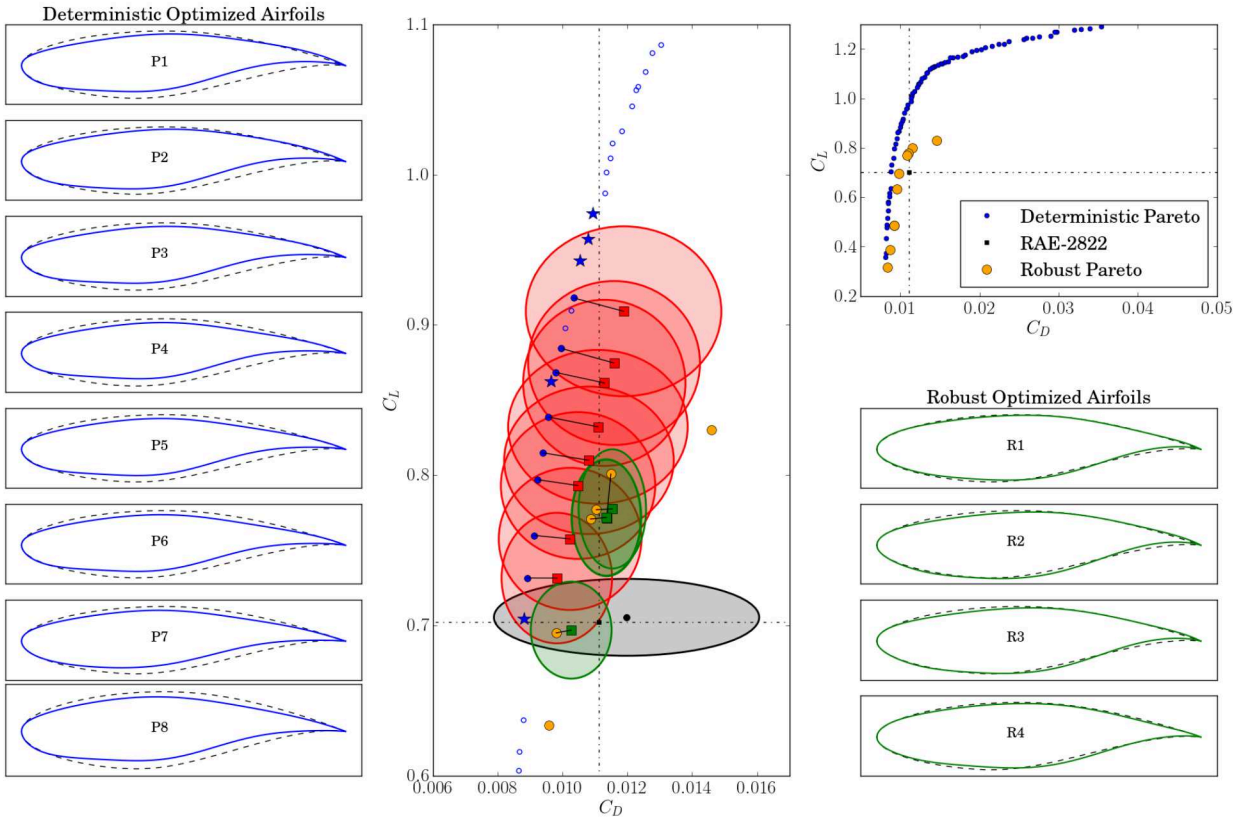

Figure 9: Deterministic and Robust Pareto fronts obtained by solving respectively the MO-DO1 and the MO-RDO1. The central plot is a blow-up view of the full Pareto. The red squares are the mean of C_L and C_D when the airfoils are operated in the uncertain environment, while the red ellipses are the dispersion around such mean values (two standard deviations). The green squares are the mean values of the robust optimal points and the green ellipses are their dispersion around such mean values (two standard deviations). Finally the black point and grey ellipse correspond to the RAE-2822 airfoil.

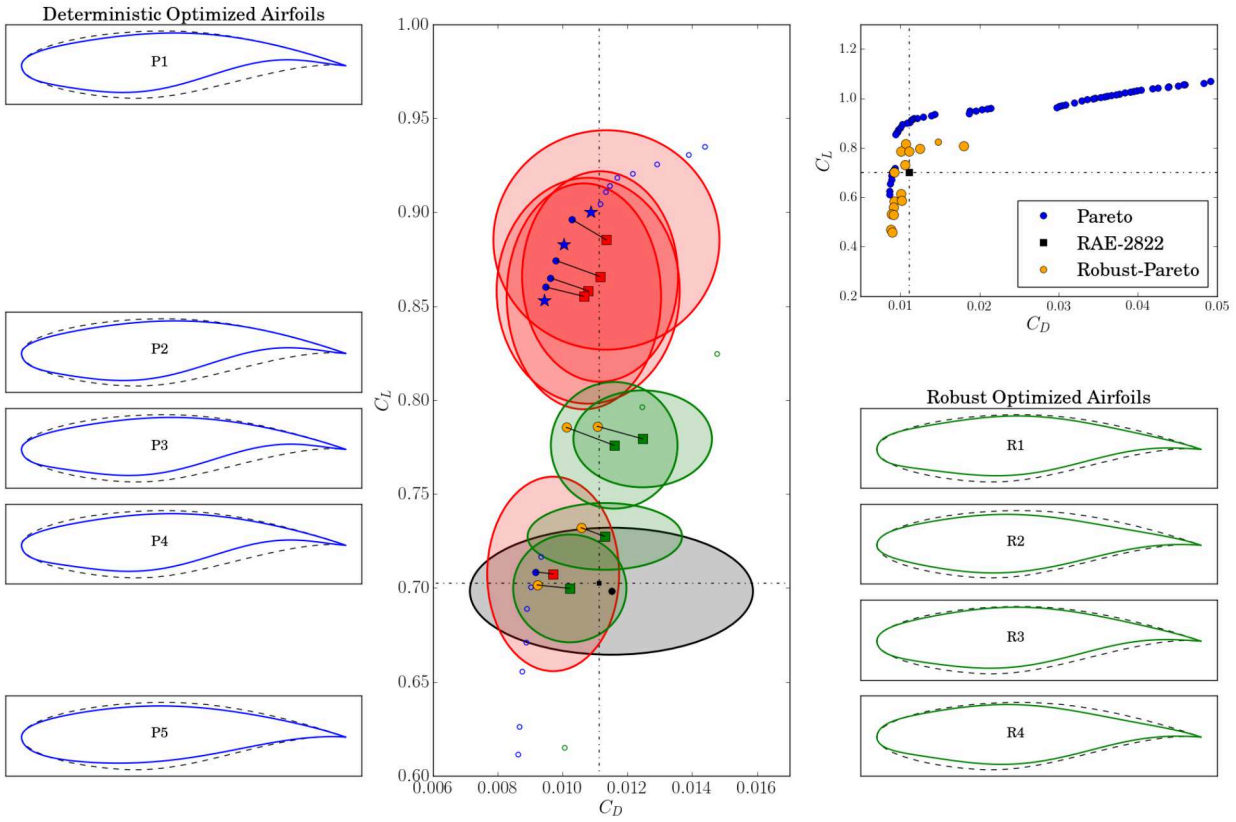

Figure 10: Deterministic and Robust Pareto fronts obtained by solving respectively the MO-DO1 (using PARSEC as design parameters) and the MO-RDO2. The central plot is a blow-up view of the full Pareto. The red squares are the mean of C_L and C_D when the airfoils are operated in the uncertain environment, while the red ellipses are the dispersion around such mean values (two standard deviations). The green squares are the mean values of the robust optimal points and the green ellipses are their dispersion around such mean values (two standard deviations).

Recent publications:

INSTITUTE of MATHEMATICS
MATHICSE Group

Ecole Polytechnique Fédérale (EPFL)

CH-1015 Lausanne

2018

01.2018 ANA SUSNAJARA, DANIEL KRESSNER:
A fast spectral divide-and-conquer method for banded matrices

02.2018 ELEONORA ARNONE, LAURA AZZIMONTI, FABIO NOBILE, LAURA M. SANGALLI:
Modelling spatially dependent functional data via regression with differential regularization

03.2018 NICCOLO DAL SANTO, SIMONE DEPARIS, ANDREA MANZONI, ALFIO QUARTERONI:
Mutli space reduced basis preconditioners for parametrized Stokes equations

04.2018 MATTHIEU MARTIN, SEBASTIAN KRUMSCHEID, FABIO NOBILE:
Mutli space reduced basis preconditioners for parametrized Stokes equations
Analysis of stochastic gradient methods for PDE-Constrained optimal control problems with uncertain parameters

05.2018 VALENTINE REY, SEBASTIAN KRUMSCHEID, FABIO NOBILE:
Quantifying uncertainties in contact mechanics of rough surfaces using the Multilevel Monte Carlo method

06.2018 MICHELE PISARONI, FABIO NOBILE, PENELOPE LEYLAND:
A continuation-multilevel Monte Carlo evolutionary algorithm for robust aerodynamic shape design

***